JACS
JOURNAL OF THE AMERICAN CHEMICAL SOCIETY

Article

pubs.acs.org/JACS

Targeting the Gatekeeper MET146 of C-Jun N-Terminal Kinase 3 Induces a Bivalent Halogen/Chalcogen Bond

Andreas Lange,[†,‡,§] Marcel Günther,[∥,§] Felix Michael Büttner,[#] Markus O. Zimmermann,[†,‡] Johannes Heidrich,[†,‡] Susanne Hennig,[†] Stefan Zahn,[¶] Christoph Schall,[#] Adrian Sievers-Engler,[⊥] Francesco Ansideri,[∥] Pierre Koch,[∥] Michael Laemmerhofer,[⊥] Thilo Stehle,[#,▽] Stefan A. Laufer,[∥] and Frank M. Boeckler*[,†,‡]

[†]Molecular Design and Pharmaceutical Biophysics, Institute of Pharmaceutical Sciences, Eberhard Karls Universität Tübingen, Auf der Morgenstelle 8, 72076 Tübingen, Germany

[‡]Center for Bioinformatics Tübingen (ZBIT), Eberhard Karls Universität Tübingen, Sand 1, 72076 Tübingen, Germany

[∥]Pharmaceutical and Medicinal Chemistry, Institute of Pharmaceutical Sciences, Eberhard Karls Universität Tübingen, Auf der Morgenstelle 8, 72076 Tübingen, Germany

[#]Interfaculty Institute of Biochemistry, Eberhard Karls Universität Tübingen, Hoppe-Seyler-Str. 4, 72076 Tübingen, Germany

[¶]Institute of Physical Chemistry, Justus-Liebig-Universität Gießen, Heinrich-Buff-Ring 17, 35392 Gießen, Germany

[⊥]Pharmaceutical (Bio)Analysis, Institute of Pharmaceutical Sciences, Eberhard Karls Universität Tübingen, Auf der Morgenstelle 8, 72076 Tübingen, Germany

[▽]Department of Pediatrics, Vanderbilt University School of Medicine, Nashville, Tennessee 37232, United States

Supporting Information

ABSTRACT: We target the gatekeeper MET146 of c-Jun N-terminal kinase 3 (JNK3) to exemplify the applicability of X···S halogen bonds in molecular design using computational, synthetic, structural and biophysical techniques. In a designed series of aminopyrimidine-based inhibitors, we unexpectedly encounter a plateau of affinity. Compared to their QM-calculated interaction energies, particularly bromine and iodine fail to reach the full potential according to the size of their σ-hole. Instead, mutation of the gatekeeper residue into leucine, alanine, or threonine reveals that the heavier halides can significantly influence selectivity in the human kinome. Thus, we demonstrate that, although the choice of halogen may not always increase affinity, it can still be relevant for inducing selectivity. Determining the crystal structure of the iodine derivative in complex with JNK3 (4X21) reveals an unusual bivalent halogen/chalcogen bond donated by the ligand and the back-pocket residue MET115. Incipient repulsion from the too short halogen bond increases the flexibility of C_ε of MET146, whereas the rest of the residue fails to adapt being fixed by the chalcogen bond. This effect can be useful to induce selectivity, as the necessary combination of methionine residues only occurs in 9.3% of human kinases, while methionine is the predominant gatekeeper (39%).

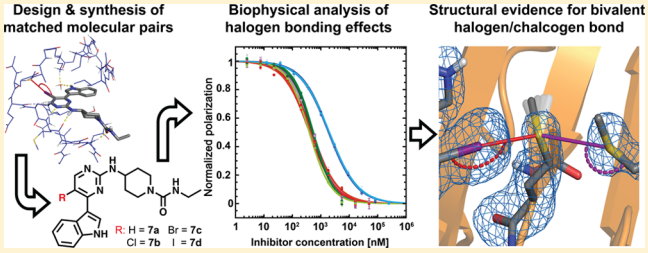

INTRODUCTION

In the past decade halogen bonding has increasingly gained attention in life sciences and drug discovery.[1−8] This attractive interaction can typically be described as a R−X···D−R′ contact, where X represents chlorine, bromine, and iodine (as electron pair acceptor) and D can be any kind of Lewis base.[9] For a broader recognition of halogen bonding in molecular design, we have recently studied halogen bonding contacts with different interaction partners in protein binding sites.[4−7] From these studies it is evident that halogen bonds can provide innovative ideas, how to access interesting parts of the biological space (e.g., therapeutic targets) from hitherto widely neglected parts of the chemical space (chemotypes featuring halogen bonds as essential key recognition motifs in the binding mode).

On the basis of the lack of directional interactions toward methionine (MET) in classical interactions, this amino acid has been particularly difficult to target, except for using hydrophobic contacts. Only recently, Meanwell and colleagues have highlighted the role of noncovalent sulfur interactions in drug design.[10] Recently, we have studied the targetability of MET by halogen bonding systematically on a quantum chemical level of theory.[4] One of our goals was to provide new insights for utilizing halogen···sulfur contacts in molecular design. Here, we

Received: July 15, 2015
Published: October 27, 2015

DOI: 10.1021/jacs.5b07090
J. Am. Chem. Soc. 2015, 137, 14640−14652

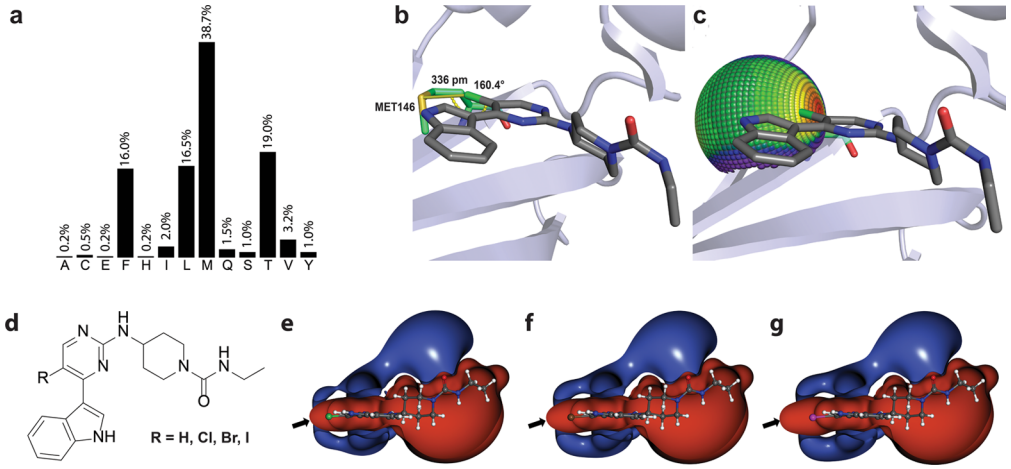

Figure 1. (a) Percentage distribution of gate keeper residues in human kinases based on kinase sequence alignments[16] obtained from http://kinase.com/human/kinome/phylogeny.html. (b) 4-{[5-Chloro-4-(1*H*-indol-3-yl)pyrimidin-2-yl]amino}-*N*-ethylpiperidine-1-carboxamide interacting with the gatekeeper MET146 of JNK3 (PDB: 2P33).[15] The chlorine···sulfur distance ($d_{X\cdots S}$ = 336 pm) and the σ-hole angle ($\alpha_{C\text{-}X\cdots S}$ = 160.4°) are depicted explicitly. (c) Data from a spherical interaction scan on the MP2/TZVPP level of theory using iodobenzene as a model ligand and dimethylsulfide as a model for methionine[4,17] were plotted onto MET146, indicating that the substitution of chlorine by iodine should be favorable (color gradient from red: very favorable to purple: unfavorable). Spherical interaction scans were prepared previously[4] by systematically rotating the ligand system around the methionine sulfur as the center of the sphere, while maintaining the orientation of the model ligand, i.e., the same σ-hole angle $\alpha_{C\text{-}X\cdots S}$. The exact spherical orientation of any ligand interacting through a halogen bond with methionine can be described by the spherical coordinates of the iodine atom (distance $d_{S\cdots X}$, azimuth and elevation angle with respect to a certain plane of symmetry of dimethylsulfide) and the σ-hole angle $\alpha_{C\text{-}X\cdots S}$. The figures in panel (b) and (c) were prepared using PyMOL.[18] (d) Structures of the designed matched molecular pair series comprising the hydrogen (**7a**), chlorine (**7b**), bromine (**7c**), and iodine derivative (**7d**). (e−g) ESP isosurfaces (MP2/TZVPP) of compounds **7b**−**d**. Negative ESP isosurfaces contoured at an energy of −0.009 au are colored in dark blue, while positive ESP isosurfaces contoured at 0.009 au are colored in red. Toward the heavier halides, the σ-hole (positive potential) on the halogen in elongation of the R−X bond (indicated by a black arrow) increases. All pictures were prepared with MOLCAD.[19,20]

target the gatekeeper MET146 of c-Jun N-terminal kinase 3 (JNK3) to exemplify the applicability of X···S halogen bonding in molecular design using computational, structural and biophysical techniques. Figure 1a shows the percentage distribution of gatekeeper residues in all human kinases. The term "gatekeeper" is commonly used to describe the residue in a kinase that blocks the hydrophobic pocket and, therefore, is a key feature of the recognition elements in the ATP-binding site of the kinase.[11] From Figure 1a, it is obvious that methionine (with ∼39%) is by far the most common gatekeeper in human kinases. It is followed by threonine (with ∼19%), leucine (∼17%), and phenylalanine (∼16%). All other amino acids together are only found in a small fraction (∼10%) as gatekeeper residues. JNK3 is a member of the mitogen-activated protein kinases (MAPK) family and a popular target for drug discovery.[12,13] Because of the lack of specific ways to target the gatekeeper methionine residue (MET146) of JNK3, traditional drug discovery approaches have focused on utilizing the side chain flexibility of this residue to shift it into a position granting access to the hydrophobic pocket.[14] However, an exhaustive PDB survey revealed that MET146 can be targeted by halogen bonding (Figure 1b,c). Actually, Alam et al. had reported a crystal structure of the complex between 4-{[5-chloro-4-(1*H*-indol-3-yl)pyrimidin-2-yl]amino}-*N*-ethylpiperidine-1-carboxamide (**7b**) and JNK3 (PDB-ID: 2P33, further referred to as 2P33), in which a chlorine is interacting with MET146.[15]

In this study, we generated the halogen/hydrogen analogues to complete the series of matched molecular pairs (Figure 1d). We used quantum chemical methods to assess the difference in V_{max}, the maximal positive electrostatic potential representing the size and strength of the σ-hole. We plotted the electrostatic potential isosurfaces of the halogenated analogues (Figure 1e−g) and optimized all four ligands in the binding pocket using TPSS-D2/SV(P). We synthesized all four ligands, establishing a new route to obtain the bromine and iodine derivatives. We expressed and purified JNK3 to characterize the differences in ligand affinities using biophysical techniques such as differential scanning fluorimetry (DSF), fluorescence polarization (FP), and isothermal titration calorimetry (ITC). Since JNK3 and p38α MAP kinase (p38α) are notoriously similar in structure, we also assessed the ligand selectivity against p38α. To elucidate the contribution of the halogen bond, we prepared the gatekeeper mutants JNK3-M146A, JNK3-M146L, and JNK3-M146T and investigated mutant-induced changes in the binding affinity compared to JNK3 wildtype (JNK3-wt) by FP competition experiment. In order to rationalize our findings, we have determined the crystal structure of JNK3-wt in complex with the iodine derivative (**7d**).

RESULTS

1. Halogen Bond Tuning (V_{max}) and Rationalization of the Designed MMPs by Quantum Chemistry. The chlorine···sulfur distance $d_{X\cdots S}$ = 336 pm and the σ-hole angle $\alpha_{C\text{-}X\cdots S}$ = 160.4° suggest that the halogen bond to the gatekeeper MET146 in 2P33 is favorable (Figure 1b). Derived from previous[4] and current theoretical work,[17] we also rationalized that the spherical geometry is beneficial (Figure 1c). The spherical geometry can be represented by the spherical coordinates (distance, azimuth, elevation) of iodine with respect to the methionine sulfur as the center of the sphere. Therefore, we generated in this study the matched molecular pairs complementing the crystallized ligand (**7b**) with the

DOI: 10.1021/jacs.5b07090
J. Am. Chem. Soc. 2015, 137, 14640−14652

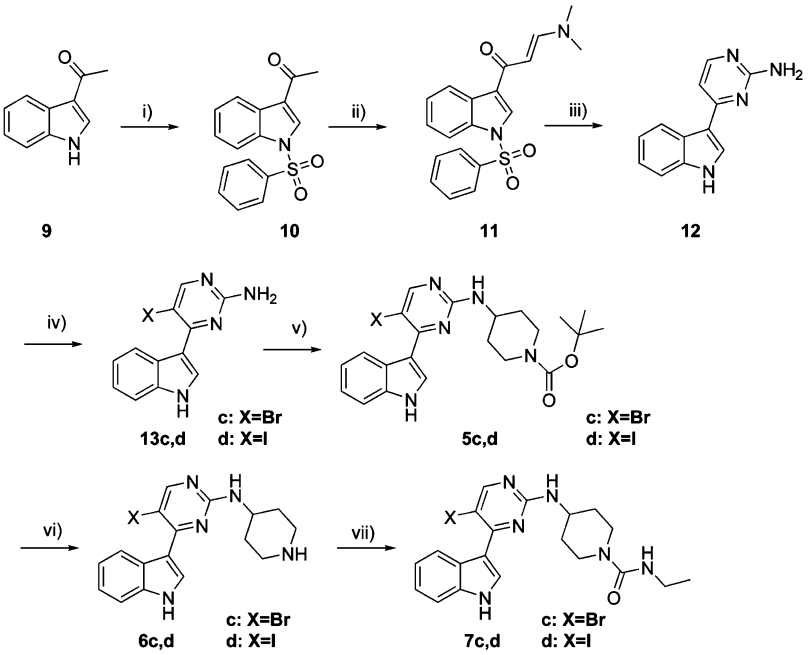

Figure 2. Synthesis of compounds **7c** and **7d**. Reagents and conditions: (i) MeOH, KOH, acetone, benzenesulfonyl chloride, rt, 92%; (ii) dimethylformamide-dimethylacetale, reflux, 24 h, 89%; (iii) MeOH, guanidine carbonate, sodium methoxide, reflux, 48 h, 61%; (iv) DMF, *N*-halosuccinimide, rt, overnight, 59−65%; (v) DCM, *N*-Boc-piperidin-4-on, sodium triacetoxy borohydride, TFA, rt, 70−80%; (vi) DCM, TFA, rt, 2 h; (vii) DCM, triethylamine, ethyl isocyanate, overnight, 40−59% (yield for step (vi) + (vii)).

analogues containing bromine (**7c**), iodine (**7d**) or hydrogen (**7a**) in position five of the pyrimidine ring (Figure 1d).

The strength of a halogen bond is tuned by the scaffold.[21−23] To elucidate this tuning effect, we calculated the electrostatic potential isosurfaces and the V_{max} value (most positive electrostatic potential on the σ-hole when mapping the ESP onto the isodensity surface) for each halogenated compound (MP2/SV(P), Figure 1e−g). **7b** appears to be hardly tuned, showing a V_{max} value of 0.123 au (chlorobenzene: 0.117 au, ΔV_{max} = 0.006 au). **7c** and **7d**, however, possess increasingly tuned σ-holes, as expected. **7c** has a V_{max} value of 0.168 au (bromobenzene: 0.150 au, ΔV_{max} = 0.018 au) and **7d** has a value of 0.219 au (iodobenzene: 0.182 au, ΔV_{max} = 0.037 au). With the V_{max} value being almost twice as large for iodine as for chlorine, a significantly stronger halogen bond should result from the proposed halogen exchange.

We further investigated, whether these tuning differences translate into changes of the binding mode. Using calculations on a TPSS-D2/SV(P) level of theory and a carefully selected binding site model to rationalize the designed MMPs. A detailed report about the protocol and results is provided in the Supporting Information. Essentially, the hydrogen bond network to the hinge binding region appeared to be intact in all compounds. The halogen bond geometry of chlorine is preserved perfectly. Despite their size, the iodine and bromine atoms in **7c** and **7d** are located 10 and 14 pm closer to the sulfur atom of MET146, respectively. This can reflect that the stronger σ-hole tuning permits a closer contact to the sulfur, but could also indicate an onset of an increasingly repulsive contact.

2. Synthesis. Compounds **7a** and **7b** were synthesized according to a route (Scheme S1) published by Alam et al.[15] with some modifications. Further details can be found in the Supporting Information. On the basis of a modified Bredereck synthesis,[24] we utilized a linear route including a pyrimidine cyclization for the synthesis of compounds **7c** and **7d** as depicted in Figure 2.

To prevent *N*-methylation during step ii, we first protected the nitrogen of commercially available 3-acetylindole as a benzenesulfonamide using already described conditions.[25] Further treatment of **10** with dimethylformamid-dimethylacetale under neat and refluxing conditions afforded **11** in high yields. The following cyclization conditions utilizing guanidine carbonate and sodium methoxide in refluxing MeOH resulted in both, the formation of the 2-aminopyrimidyl product **12** including the cleavage of the benzenesulfonamide group in the same step in acceptable yields. According to Rossignol et al.[26] 2-amino-4-indolylpyrimidines can be regioselectively halogenated using *N*-halosuccinimides in polar solvents. It is noteworthy that we isolated **5c** and **5d** in moderate yields without the occurrence of regioisomeric halogenated side products under the depicted conditions in contrast to our attempts in halogenating **3a** or **4a** (Scheme S1, Supporting Information), suggesting a crucial role of the primary 2-amino group in selective electrophilic halogenation. The 2-aminopyrimidines **13c** and **13d** can be smoothly converted into the secondary amines **14c** and **14d** via reductive amination in DCM using TFA as acid and sodium triacetoxy borohydrid as reducing agent at room temperature without cleavage of the Boc protective group or reductive dehalogenation.[27] Again, we used 20% TFA in DCM to quantitatively remove the Boc group from the 4-aminopiperidino side chain and successfully introduced the urea structure via electrophilic addition to ethyl isocyanate under basic conditions in DCM at room temperature to yield **7c** and **7d** in moderate overall yields.

3. Biophysical Characterization. *3.1. Fluorescence Polarization (FP) Assay.* We used a fluorescence polarization assay as the primary biophysical method to determine K_I values for **7a−d**. When suitable fluorescent reporter molecules are available, the FP assay is an elegant, rapid, and dependable

DOI: 10.1021/jacs.5b07090
J. Am. Chem. Soc. 2015, 137, 14640−14652

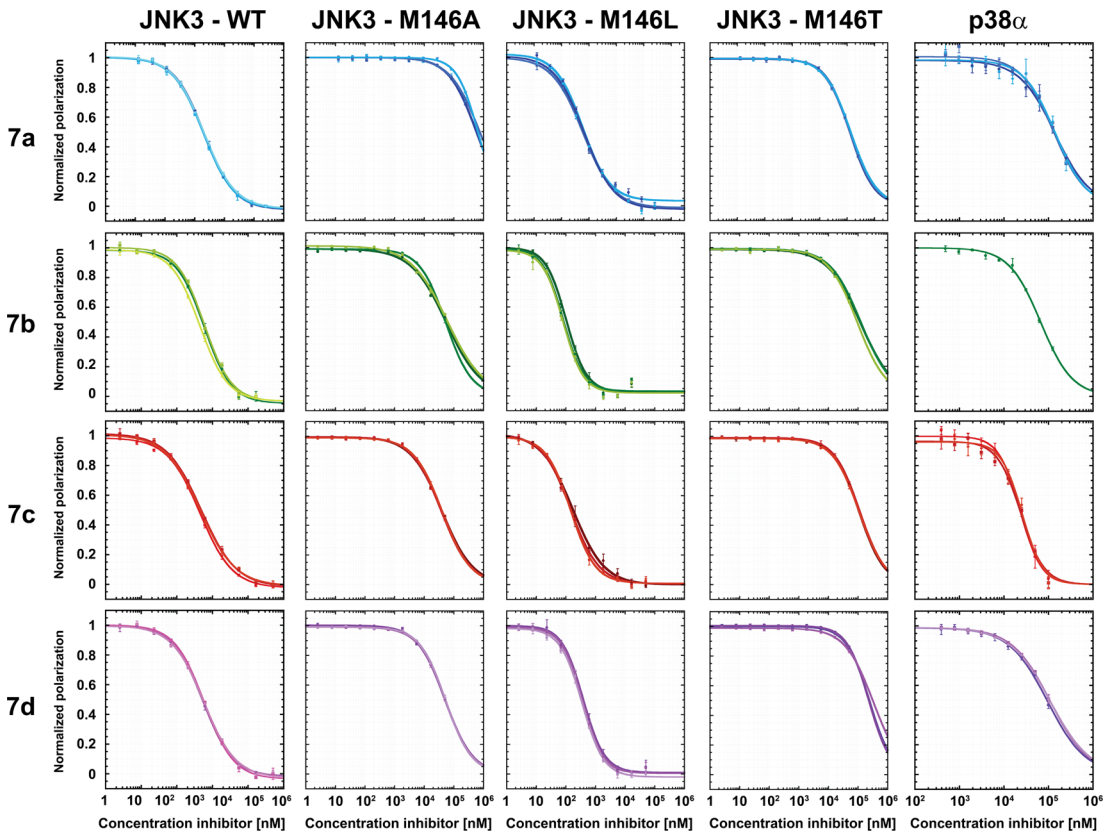

Figure 3. Fluorescence polarization-based competition binding experiments using compounds **7a**–**7d** and JNK3-wt, the JNK3 mutants M146A, M146L, and M146T, or p38α. The polarization signal (in mP units) was read using a BMG CLARIOstar reader. The values were normalized to a range from 100% to 0% polarization. Eleven concentrations of the respective inhibitor were measured in quadruplicate and each competition binding experiment was repeated three times, except for **7b** with p38α, where limited compound availability allowed only one experiment. Because of the onset of ligand precipitation, concentrations >100 μM were neglected and removed from the plot. The four parameter logistic nonlinear regression model was used for all curve fits. For JNK3-M146A and JNK3-M146T the asymptote for full displacement was fixed to 0% normalized polarization. Plots were prepared using KaleidaGraph.[33]

Table 1. Results of the Normalized FP-Assay for JNK3 and p38α

	JNK3					JNK3-wt preference			
	wt	M146A	M146L	M146T	p38α				
compound	K_D [nM]	K_D [nM]	K_D [nM]	K_D [nM]	K_D [nM]	K_D (M146A)/ K_D (wt)	K_D (M146L)/ K_D (wt)	K_D (M146T)/ K_D (wt)	K_D (p38α)/ K_D (JNK3-wt)
PIT0105016[a]	4.0 ± 0.2	2.3 ± 0.2	31 ± 3.5	3.0 ± 0.2	n.d.	0.58	7.8	0.75	–
RN4646[b]	n.d.	n.d.	n.d.	n.d.	7.3 ± 1.3	–	–	–	–
7a[c]	270 ± 7.9	56000 ± 6000[e]	270 ± 15	14000 ± 470[e]	27000 ± 1100	210	1.0	52	100
7b[c]	68 ± 9.1	4800 ± 230[e]	31 ± 4.6	12000 ± 1400[e]	14000[d]	71	0.46	180	210
7c[c]	58 ± 2.3	3300 ± 100[e]	61 ± 5.5	12000 ± 280[e]	4800 ± 220	57	1.1	210	83
7d[c]	72 ± 2.5	4500 ± 96[e]	160 ± 5.6	28000 ± 4400[e]	21000 ± 1300	63	2.2	390	290

[a]PIT0105016 is a novel fluorescein-labeled, pyridinylimidazole-based high-affinity probe for JNK3.[31] [b]RN4646 is a fluorescein-labeled analogue of SB203580.[30] K_D values of both reporter ligands were determined by three independent direct titrations with 12 concentrations of protein measured in quadruplicate. [c]The K_D values have been determined by three individual competition binding assays with 11 compound concentrations measured in quadruplicate. K_D values were derived using the K_I calculator of Shaomeng Wang and co-workers (http://sw16.im.med.umich.edu/software/calc_ki/).[32] [d]Because of the limited availability of **7b**, p38α affinity was only determined as a single measurement of 11 concentrations of **7b** in quadruplicate. [e]Because of low affinities and limited compound solubility of **7a**–**d**, no complete displacement of the reporter ligand could be observed. The normalization was, therefore, done by using the average FP values of the reporter ligand in buffer as the expected minimum of the curve. From the other experiments we can deduce that the given K_D values are the lower limit of the possible values obtainable from curve fitting.

method to assess a broad range of affinities (over several orders of magnitude).[28,29] On the basis of a previously reported fluorescein-labeled analogue of SB203580[30] (RN4646) as a high-affinity fluorescent probe for p38α (K_D of 7.3 nM) and a novel fluorescein-labeled, pyridinylimidazole-based high-affinity probe for JNK3 (PIT0105016, K_D of 4.0 nM),[31] we were able to determine both, affinities and selectivities, with good precision. Figure 3 shows the curve fits of three individual competition binding experiments per compound for **7a**–**d**. Every individual curve is based on 11 concentrations, each

DOI: 10.1021/jacs.5b07090
J. Am. Chem. Soc. 2015, 137, 14640–14652

measured in quadruplicate. Mean values and standard deviations for the K_D values were obtained by three individual direct titrations of the reporter compounds (PIT0105016 and RN4646) and the K_I values of **7a−d** were obtained by three individual competition experiments (Table 1).

For JNK3 (wt = wildtype), well-defined, reproducible sigmoidal curves were obtained, showing only small standard deviations for each concentration measured in quadruplicate. **7c** exhibits the highest affinity with a K_I of 58 nM, followed by **7b** with 68 nM, and **7d** with 72 nM. For the unsubstituted ligand **7a**, a K_I value of only 270 nM is obtained. According to ANOVA applying the Bonferroni post hoc test, the difference between **7a** and all other ligands is highly significant ($p < 0.0001$); however, the results for **7b−d** are not significantly different. Consistent with our QM-based analysis of the proposed interactions and previous DSF experiments (see Supporting Information: Figure S3 and Table S3), there is little difference between **7c** and **7d**. In addition, all halogenated ligands exhibit better binding to JNK3 than **7a**. However, it is surprising that **7b** seems to have the same affinity for JNK3 as **7c,d**.

We tested **7a−d** on p38α, as well, to evaluate similarities and differences in JNK3 selectivity. JNK3 and p38α are both MAPK kinases, showing a sequence identity of 51% and substantial three-dimensional similarity, particularly in the binding site.[14] Still, some crucial residues in the binding site are well-known for inducing selectivity. For example, the gatekeeper in JNK3 is a methionine (MET146), whereas in the p38α the gatekeeper is a threonine (THR106). Another important difference between these two proteins is located in the hinge region, where ASP150 in JNK3 corresponds to GLY110 in p38α, which facilitates a flipped conformation in the hinge that can be used to obtain highly selective ligands for p38α.[34] According to DSF experiments with p38α, we expected to find only weak binding (see Supporting Information). The results are given in Figure 3 and summarized in Table 1. On the basis of the decrease of affinity for p38α, we had to increase the ligand concentration up to 200 μM. We encountered that limited solubility of all compounds under the given buffer conditions at concentration higher than 100 μM leads to an onset of precipitation. Consequently, these concentrations were removed from the normalized plots. To still provide a reasonable curve fitting to the remaining data, we normalized the fluorescence polarization using the polarization of the labeled compound alone in buffer (~70 to 50 mP) as the lowest possible value. **7a** is the weakest binder (27 μM), followed by **7d** (21 μM) and **7b** (14 μM). Interestingly, **7c** shows the highest affinity for p38α with a K_I value of 4.8 μM. According to ANOVA applying the Bonferroni post hoc test, all measured K_I values are different with high statistical significance ($p < 0.005$). In the case of **7b** only one independent experiment could be conducted based on substance limitations. Thus, assessment of statistical significance is invalid in this case.

To evaluate the contribution of the σ-hole interaction of the halogens with the gatekeeper residue M146 to the observed structure-affinity relationships, we exchanged methionine into alanine, leucine, and threonine by side-directed mutagenesis. Expression and purification of all mutants was done as for JNK3-wt. Confirmation of the correct mutation was obtained by plasmid sequencing (GATC) and determination of the molecular mass of the mutant protein by ESI-MS. JNK3-M146A was used as control for the loss of the direct interaction (σ-hole bond or other) with methionine. The affinity of the halogenated ligands **7b−d** is reduced by a factor of 57-fold to 71-fold (Table 1), while the unsubstituted ligand **7a** even suffers a 210-fold loss in affinity. Because of the limited solubility of all compounds and the increased affinity of the fluorescence reporter PIT0105016 for JNK3-M146A, the highest concentration of the compounds displaced PIT0105016 by only up to 50%. Therefore, the fluorescence polarization signal of PIT0105016 in buffer was used as the target value for full displacement of PIT0105016 and the asymptote for full displacement was fixed to 0% normalized polarization when performing the curve fit using a four parameter logistic nonlinear regression model (Figure 3). In the context of all other FP experiments, it can be deduced that the K_D values obtained for JNK3-M146A are at the lower limit of the values expectable without the given intrinsic compound property limitations. The overall size of the affinity loss is very well in line with the importance of the gatekeeper interactions, whether they are based on σ-hole bonding or not.

With 16.5%, leucine is one of the most frequent gatekeeper residues found in the human kinome. It has a rather similar size compared to methionine, however, lacking electron pair donor functions, it cannot engage in σ-hole bonds. Thus, JNK3-M146L was prepared as an interaction-specific control, indicating possible changes in the selectivity profile in human kinases. As expectable, **7a** did not show any affinity difference for JNK3-M146L versus JNK3-wt. However, there is a clear differentiation for the halogenated ligands: Bromine (**7c**) shows no significant difference (K_D = 61 nM), while chlorine (**7b**) benefits with statistical significance (2.2-fold; $p < 0.01$; K_D = 31 nM) from the exchange into leucine. In contrast, iodine binds with significantly less affinity to JNK3-M146L (K_D = 160 nM), resulting in a 2.2-fold preference for JNK3-wt ($p < 0.001$). A plausible explanation of this observation is that several dispersive CH-X interactions onto the negative electrostatic potential of the halogen can compensate for the loss of the halogen bond. For the smaller chlorine, these can even overcompensate the effect of the halogen bond, while bromine is indifferent and the potential repulsion of the larger iodine leads to a reduced affinity. This data highlights that, although there is a plateau of affinity in this ligand series, the type of halogen (Cl, Br, I) actually has an important influence on the selectivity profile.

The JNK3-M146T mutant was prepared as link between JNK3 and p38α. In addition, threonine is the second most frequent gatekeeper residue (19%) in human kinases. Thus, this control provides important information about the extended selectivity profile. The affinities obtained for JNK3-M146T closely resemble the data obtained for p38α, as we expected. In contrast to the M146A mutant, **7a** shows a smaller decrease in affinity (52-fold, K_D = 14 μM), whereas **7b−d** prefers JNK3-wt by a factor of 180-fold (**7b**) to 390-fold (**7d**). This strong affinity loss for all halogenated compounds implies that no alternative halogen bond can be formed onto the threonine oxygen. We also conclude that the interaction toward the gatekeeper residue threonine is the most influential parameter for p38α/JNK3 selectivity. Similar to the M146A mutant, the fluorescence reporter PIT0105016 could not be fully displaced by increasing concentrations of **7a−d**. Nevertheless, we can infer from other experiments that the given K_D values (obtained by setting the asymptote for full displacement of PIT0105016 to the fluorescence polarization of PIT0105016 in buffer) represent the lower limit of the possible K_D values.

DOI: 10.1021/jacs.5b07090
J. Am. Chem. Soc. 2015, 137, 14640−14652

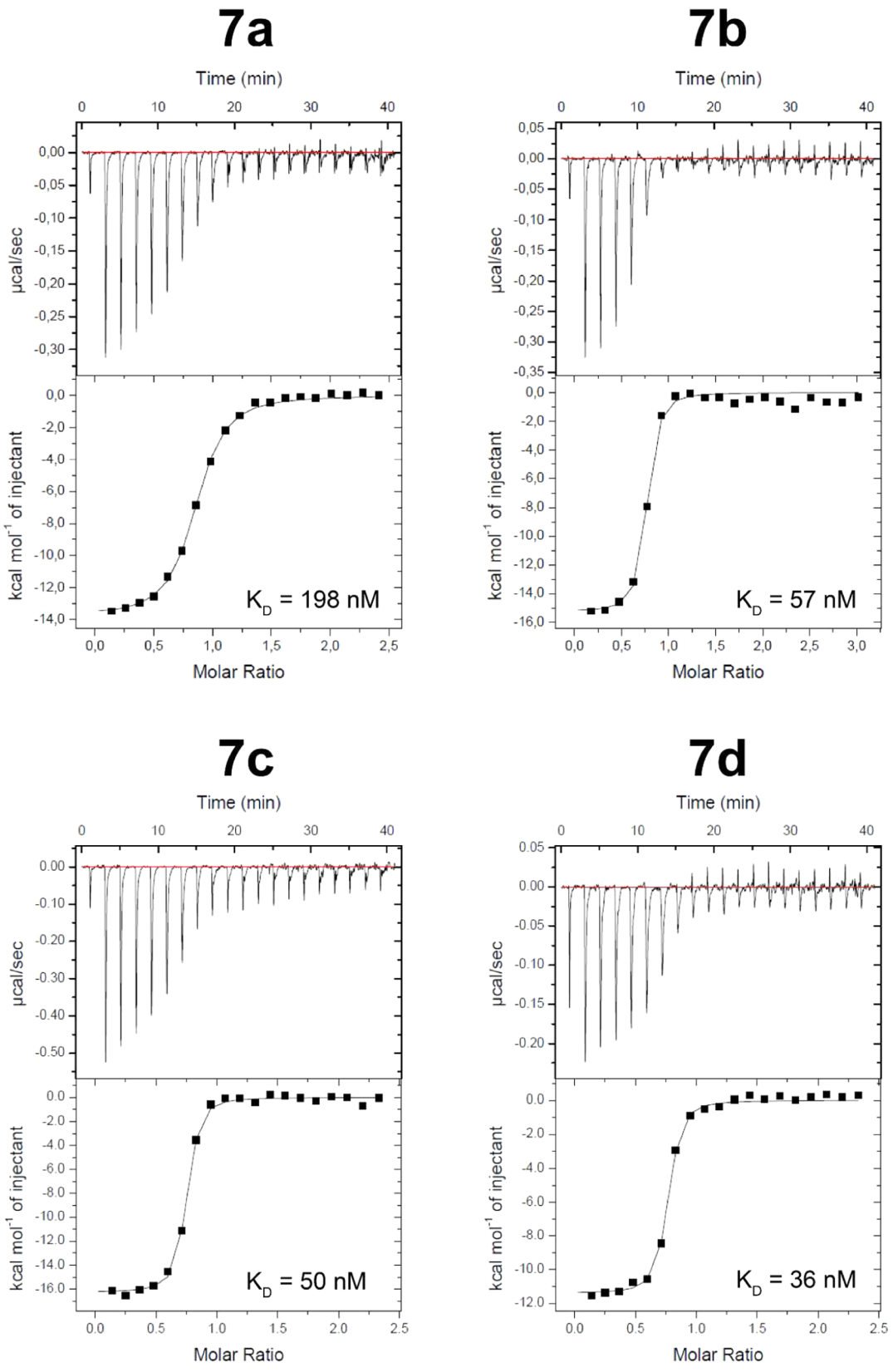

Figure 4. Results of the reverse ITC experiment. Protein concentration was 115 μM and compound concentration was 10 μM (for **7a**, **7c**, and **7d**) and 8 μM (for **7b**).

The FP-assay clearly confirms moderate to good JNK3 selectivity in the investigated compounds, similar to the DSF data. Using the point mutations M146A, M146L and M146T, we have shown that (a) the gatekeeper contact is important for maintaining good kinase affinity, (b) threonine as a gatekeeper is not able to accept a halogen bond with its hydroxyl oxygen atom, (c) threonine is also not able to engage in any other alternative, attractive interaction (neither dispersive/hydro-

DOI: 10.1021/jacs.5b07090
J. Am. Chem. Soc. 2015, 137, 14640−14652

Table 2. Results of the ITC Measurements of the Compounds with JNK3

	N	K [M^{-1}]	K_D [nM]	c-value	ΔH [kcal·mol^{-1}]	ΔS [cal·mol^{-1}K^{-1}]
7a	1.20	5.06×10^7	198 ± 28	60	−10.7 ± 0.5	−5.12 ± 2.04
7b	1.39	1.75×10^7	57 ± 5	180	−11.3 ± 0.5	−4.95 ± 1.50
7c	1.48	2.00×10^7	50 ± 7	300	−10.3 ± 1.1	−1.17 ± 3.58
7d	1.36	2.80×10^7	36 ± 7	380	−8.3 ± 0.7	6.13 ± 2.10

phobic, nor polar) to compensate for the loss of interaction, (d) not only halogen bonds, but also dispersive/hydrophobic interactions can preserve ligand affinity, however, (e) leucine differentiates between the halogens, preferring the small chlorine featuring a less pronounced σ-hole over the large iodine with a strongly pronounced σ-hole. As a consequence, halogen bonds by different halogens can affect not only affinity, but also selectivity, making them interesting tools for kinase drug discovery.

3.2. Isothermal Titration Calorimetry (ITC). Using isothermal titration calorimetry, we aimed for an independent technique with a complementary biophysical readout in order to confirm our findings in the FP-assay and to resolve the binding constants into their thermodynamic parameters. We optimized the titration protocol to obtain well-defined binding isotherms with suitable c-values for **7a**−**d** in the range of 60 to 380. Under these conditions both, K_D and ΔH, can be derived from the binding isotherm with good reliability.[29] To achieve this, we had to apply a reverse ITC setup, based on the lack of solubility of the halogenated compounds. The sample cell was filled with a solution of **7a**−**d** in buffer containing 5% DMSO (at a concentration of 8−10 μM). A JNK3 protein solution in buffer containing 5% DMSO (at a concentration of 115 μM in the syringe) was titrated into the sample cell. Raw data and the corresponding binding isotherms of a characteristic titration experiment for each ligand are presented in Figure 4. Statistics for the relevant thermodynamic parameters from four independent titrations per compound are summarized in Table 2.

The K_D values obtained by ITC are in good agreement with the affinities measured in the FP-assay. Small differences between the ITC and FP results might arise from the intrinsic characteristics of both biophysical techniques/experimental protocols (direct binding vs competition experiment, equilibration times, titration vs simultaneous measurement of all concentrations, solubility-based errors, etc.), as well as from differences in the buffer conditions (2 mM TCEP for ITC experiments vs 10 mM β-mercaptoethanol for FP experiments).

While **7a** binds clearly weaker (198 nM) than any of the halogenated compounds, there seems to be a slight trend toward better affinities for the heavier halogens (57 nM for **7b**, 50 nM for **7c**, and 36 nM for **7d**). However, by applying one-way ANOVA with Bonferroni post hoc testing, it becomes evident that there is no statistical significance in the different K_D values found for **7b**−**d**. Only **7a** is different to all other compounds with high statistical significance ($p < 0.0001$). Thus, we conclude that the insignificant difference found with both methods for **7b**−**d** clearly show that for this series of matched molecular pairs, no gain of affinity can be induced by replacing chlorine by the heavier halides. Interestingly, there is also no apparent loss of affinity.

Decomposition of the free energy of binding into enthalpy (ΔH) and entropy ($-T\cdot\Delta S$) contributions, however, draws attention to some important differences between **7b**, **7c**, and **7d**. The enthalpy decreases from −11.3 kJ/mol for the chlorine derivative **7b** to −10.3 kJ/mol for the bromine derivative **7c**, and −8.3 kJ/mol for the iodine derivative **7d**. On the basis of the slightly higher standard deviation for bromine, ANOVA with Bonferroni post hoc analysis clearly shows that only the difference between **7d** and the others is significant ($p < 0.015$). Considering that iodine could in principle form a much stronger halogen bond than bromine or chlorine, this result is at least surprising. To elucidate the reason for this behavior, we solved the crystal structure of **7d** in complex with JNK3.

From Table 2, it is also evident that for the heavier halides the entropic contribution to the free energy of binding becomes more favorable, compensating almost exactly the loss of enthalpy. Thus, although ΔG is hardly affected by the type of halogen forming the halogen bond to MET146, the thermodynamic parameters are clearly deviating between chlorine, bromine, and iodine. Similar to ΔH, ANOVA with Bonferroni post hoc testing showed a significant difference in ΔS only between iodine (**7d**) and the other compounds ($p < 0.01$), which again might be attributed to the high standard deviation of **7c**. A summary plot of ΔH, $-T\cdot\Delta S$, and ΔG highlighting the enthalpy−entropy compensation in **7b**−**d**, can be found in the Supporting Information (Figure S4).

We likewise tried to perform ITC experiments with **7a**-**d** and p38α. However, because of the limited solubility of the compounds and their weak binding to p38α, neither direct nor indirect titration experiments yielded satisfying c-values and interpretable binding isotherms.

4. Crystal Structure of 7d in Complex with JNK3 (4X21) and its Comparison to 2P33. In order to find possible explanations for the significantly different thermodynamics of **7d**, we have solved the structure of **7d** soaked into a JNK3 crystal at a resolution of 1.95 Å with a final R_{work}/R_{free} of 19.86/22.30 (PDB code 4X21; for further refinement statistics see Table 3). During model building, it was not possible to trace the peptide chain between ALA211 and VAL225, as well as ILE375 and ASP391 due to lack of electron density. Poorly defined electron densities for these comparatively flexible loops were also encountered in previous crystal structures of JNK3.[14,35,36]

The crystals contain two structurally very similar copies of ligand-bound JNK3 in their asymmetric unit. Because of the higher overall B-factors in chain B, we will first describe the binding situation of chain A. Although we provide comparisons and measurements on the pm scale, it should be emphasized that the possible coordinate error of the crystal structure (Table 3) certainly limits the interpretability of the very small differences sometimes observed. Therefore, we have additionally performed some accompanying calculations to elaborate on the meaning of the observed trends. Figure 5a shows that **7d** binds tightly to the hinge region and forms a halogen bond to MET146. The hydrogen bond distance to the hinge region is 205 pm for N···NH and 206 pm for NH···OC. This slightly exceeds the predicted values by 20 or 14 pm, respectively (see Table S1). In contrast, the CH···OC weak hydrogen bond involving the GLU147 backbone was found to be 241 pm long,

DOI: 10.1021/jacs.5b07090
J. Am. Chem. Soc. 2015, 137, 14640−14652

Table 3. Crystallographic Data and Refinement Statistics for 4X21

Data Collection	
Beamline	HZB-BESSYII BL14.1
Space group	$P2_12_12$
Cell dimensions (Å)	a = 155.94 b = 109.84 c = 43.91 $\alpha = \beta = \gamma = 90°$
Wavelength (Å)	0.918409
Resolution (Å)[a]	50.0−1.95 (2.00−1.95)
Measured reflections	741250 (55236)
Unique reflections	56051 (4113)
CC1/2[a]	99.9 (67.9)
Completeness (%)[a]	100 (100)
Redundancy[a]	13.2 (13.4)
$I/\sigma(I)$[a]	14.35 (2.42)
Refinement	
Resolution (Å)	46.89−1.95
R_{work}/R_{free}[b]	19.86/22.30
Number of atoms	5595
Protein	5195
Water	344
7d	56
B-factors (Å^2)[c,d]	
Protein	35.7 (13.9−79.4)
Water	38.6 (16.3−61.9)
7d	36.3 (24.7−49.1)
r.m.s.d.	
Bond length (Å)	0.014
Bond angles (deg)	1.241
Ramachandran Plot	
most favorable (%)	98.5
allowed (%)	1.5

[a]Values in parentheses are for the highest-resolution shell. [b]R_{free} represents a 5% subset of the total reflections, that are excluded from refinement. [c]The overall mean B-factor is found to be in good agreement with the Wilson B-factor. [d]The overall coordinate error was calculated as approximately 0.2 Å.

as predicted by the QM model. The iodine···sulfur distance $d_{I\cdots S}$ in chain A is with 315 pm rather short, featuring an excellent σ-hole angle of 170.3°. Thus, our prediction (319 pm/165°) closely matches the experimentally found parameters. The ligand in chain B binds in an almost identical mode to JNK3 (see Figure S5). The hydrogen bonds to the hinge in chain B have a length of 204 pm (N···NH) and 215 pm (NH···OC), deviating by only 1 and 9 pm from chain A. The distance of the weak hydrogen bond in chain B ($d_{CH\cdots OC}$ = 234 pm) also closely matches chain A. The halogen bond has a distance of only 305 pm and a σ-hole angle of 168.4°. The deviation of the σ-hole angle is only marginal and the shortening of $d_{I\cdots S}$ by 10 pm appears small. Still, this very short contact can be actually detrimental for the energy of the system. Indeed, as demonstrated in Figure 5d, the attractiveness of the interaction is further decreased at a distance of 305 pm. However, this very short length can also be explained by significant radiation damage to the iodine of **7d** in chain B. In addition, there is also a small change in the geometry of the residues lining the binding site, caused by a crystallization interface in chain A and another in chain B. We provide a detailed account of these structural changes and their effect on the ligand binding in the Supporting Information (Figure S7). It should be noted that in chain B, the electron density of the *N*-ethylcarboxamide moiety is more clearly defined, confirming that the 180° flipped orientation of the ethyl group in comparison to the structure of **7b** in 2P33 is likely favored.

Figure 5b shows chain A (orange) superposed onto the crystal structure of 2P33 (cyan). Both share an almost identical binding mode. The hydrogen bonds to the hinge in chain A of 4X21 only deviate by 2 pm (N···NH) and 9 pm (NH···OC) from 2P33. The distance of the weak hydrogen bond (CH···OC) is likewise altered by 3 pm only. The difference in the hinge binding geometry, thus, appears negligible. The halogen bond of the iodine in 4X21 is 21 pm shorter than for chlorine and the σ-hole angle improves by ∼10° to an almost linear arrangement. While the small deviation of the σ-hole angle is almost optimal, the significantly shorter $d_{I\cdots S}$ could imply an improved, tighter binding, but could also represent a repulsive contribution. Similar to **7b**, **7d** binds to LYS93 via an interstitial water molecule. The hydrogen bond network around LYS93 in 4X21 appears to be slightly extended by another water molecule, defined with good electron density and a low B-factor.

In summary, the comparison of both crystal structures demonstrates that **7d** and **7b** are both tightly bound by their hydrogen bonding network involving the hinge region (GLU147, MET149) and the bridged interaction with LYS93. From the QM-based prediction we inferred that the indole-substituted 2-aminopyrimidine scaffold will not shift significantly to accommodate the larger iodine, because the stronger σ-hole of iodine leads to a decreased halogen bond length of 319 pm, in comparison to 333 pm for chlorine. Despite a reasonably good consistency between our QM-model and the crystal structure (see Table S1), we deemed it interesting that the halogen bond length for chlorine (**7b**) was predicted to be slightly shorter, while the length for iodine (**7d**) was predicted to be slightly longer than in the crystal structure.

5. Bivalent, Mixed Halogen and Chalcogen Bonding and Torsional Flexibility of the MET146 χ_3 Dihedral Angle $\delta_{C\beta\text{-}C\gamma\text{-}S\text{-}C\varepsilon}$. In order to analyze the relative strength of the experimentally found halogen bond with a distance of 315 pm, we employed QM calculations on a TPSS-D2/TZVPP level of theory including the entire ligand **7d** together with the capped methionine (cMET146 = 2-acetamido-*N*-methyl-4-(methylthio)butanamide). We also used this model system to determine another crucial parameter: During refinement of the crystal structure 4X21, the electron density of the C_ε of MET146 is not as well-defined as the rest of the residue. The electron density map for the neighbor atom sulfur is spherically elongated, making two alternative, preferential orientations of the terminal C_ε most plausible. It should be noted that the lack of electron density for this atom clearly indicates a higher flexibility, which might be connected to the stronger entropy contribution to binding of **7d**, which we observed in ITC experiments.

Even more importantly, the orientation of C_ε is of utmost importance for the strength of the halogen bond.[4] The highest electron densities (of the "lone pairs") are found almost perpendicular to the plane defined by C_γ, S, and C_ε, located above and below the sulfur. In plane, the sulfur exhibits σ-holes of itself, efficiently preventing a halogen bond to be formed in this orientation. Thus, the MET146 χ_3 dihedral angle $\delta_{C\beta\text{-}C\gamma\text{-}S\text{-}C\varepsilon}$ has an essential influence on the energy evaluation of the system. From the experimental electron density, we concluded that the most likely dihedral angle is $\delta(C_\beta{-}C_\gamma{-}S{-}C_\varepsilon) = -95°$.

DOI: 10.1021/jacs.5b07090
J. Am. Chem. Soc. 2015, 137, 14640−14652

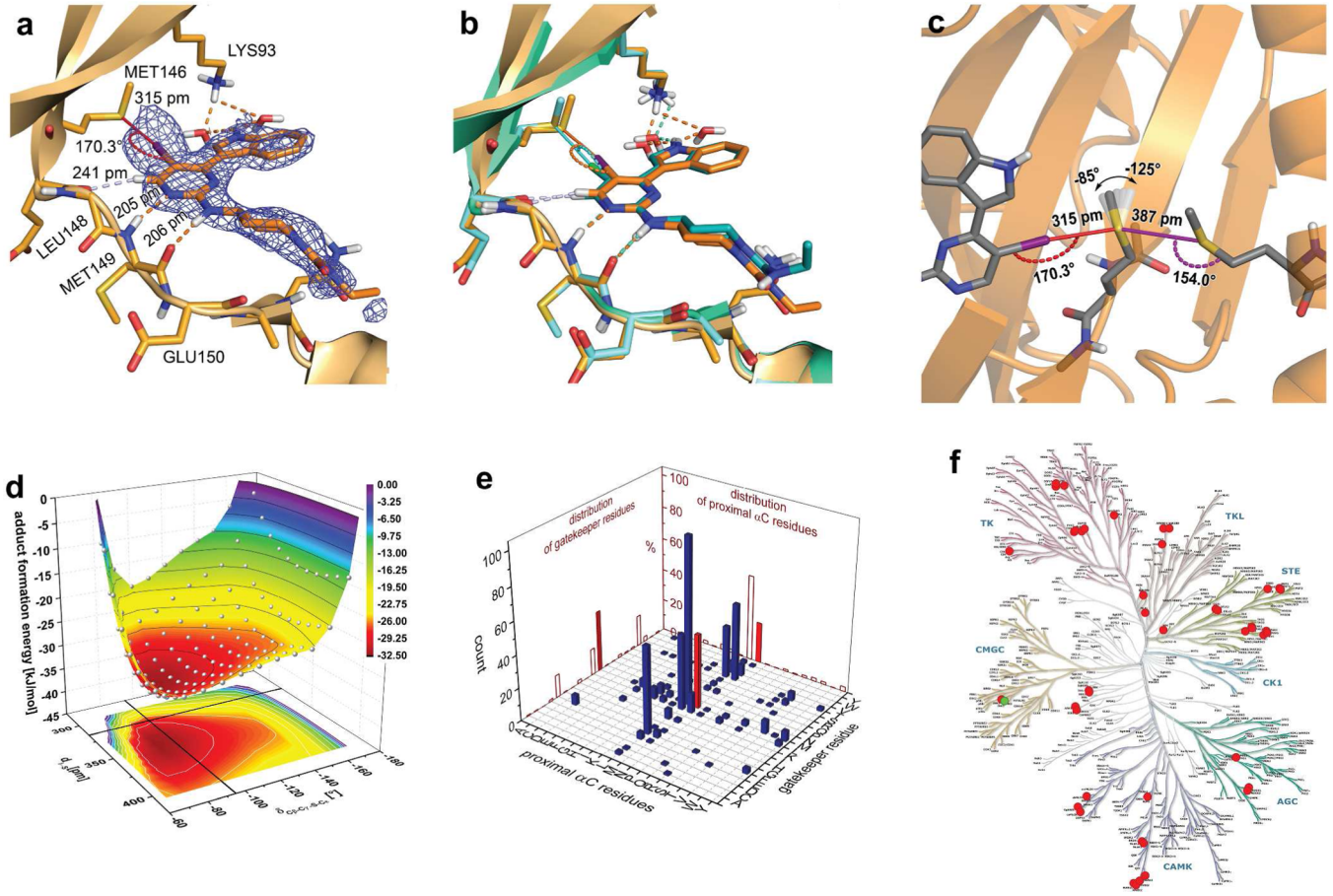

Figure 5. Crystal structure of the 5-iodopyrimidine derivative (**7d**) in complex with JNK3 and computational analysis of the iodine···sulfur halogen bond. (a) The binding site of chain A of 4X21 is presented with emphasis on the tight hydrogen bond network toward the hinge region and via two bridging water molecules toward LYS93. The protein is shown as a bright orange cartoon representation, with selected residues in the cavity depicted as stick models. The ligand is shown as an orange stick model, and hydrogen bonds are highlighted with broken, orange lines. The weak hydrogen bond (C—H···O═C) involving GLU147 is indicated by light blue, broken lines. The halogen bond targeting the gatekeeper MET146 is shown as a red line, while the σ-hole angle is depicted as a curved, dotted, red line. Characteristic distances and the σ-hole angle are denoted explicitly (see also Table S1). An unbiased simulated-annealing omit electron-density map ($F_o - F_c$) for the ligand is shown at a contour level of 3.0 σ. Only density within a maximal distance of 220 pm of any atom of the ligand is displayed for clarity reasons. The *N*-ethyl-substituent of the piperidinyl-1-carboxamide moiety of 7d protruding from the cavity was not clearly resolved in the crystal structure. (b) Overlay of chain A of 4X21 (bright orange) and 2P33 (bright cyan). The respective ligands **7d** of 4X21 and **7b** of 2P33 are colored in orange and cyan. The polar interactions (hydrogen, weak hydrogen and halogen bonds) are depicted similar to panel (a). For better differentiation between the structures, the color code of the ligands is likewise used for the interactions. Alignment and superposition has been done in MOE.[37] Pictures have been prepared and rendered in PyMOL.[18] (c) MET146 is engaged in a bivalent halogen bond (red) and chalcogen bond (purple) donated by **7d** and MET115, respectively. Distances ($d_{I\cdots S}$ and $d_{S\cdots S}$) and σ-hole angles ($\alpha_{C\text{-}I\cdots S}$ and $\alpha_{C\gamma\text{-}S\cdots S}$) characterizing the quality of the interactions are depicted in the model system (shown as sticks). This consists of **7d** and the two capped methionine residues (cMET = 2-acetamido-*N*-methyl-4-(methylthio)butanamide) in position 146 and 115. The flexibility of the χ_3 dihedral angle ($\delta_{C\beta\text{-}C\gamma\text{-}S\text{-}C\varepsilon}$) is represented by partially transparent replicas of the C_ε-S bond of MET146. (d) The depicted 3D plot shows the results (white dots) of the systematic variation of $\delta_{C\beta\text{-}C\gamma\text{-}S\text{-}C\varepsilon}$ in increments of 10° and $d_{I\cdots S}$ between 295 and 405 pm in steps of 10 pm. Adduct formation energies (in kJ/mol) were calculated on a TPSS-D2/TZVPP level of theory by subtracting the DFT-energy of the three educts (**7d**, cMET146, and cMET115) from the DFT-energy of the complex. Fitting a surface to the data, which was color coded with a gradient representing the adduct formation energies, and projection of the energy profile onto the *xy*-plane was done in Origin9.1.[38] The point of intersection between the two black lines plotted in the projected map indicates the most reasonable experimental geometry. (e) 3D bar chart depicting the number of human kinases for each possible combination of gatekeeper residue and their proximal residue in the αC-helix. Residues were identified and statistics derived based on kinase sequence alignments[16] obtained from http://kinase.com/human/kinome/phylogeny.html. Red 2D bar charts projected onto the side and back of the 3D plot provide the relative overall distribution of residues for both positions in 486 human kinases. The red 3D bar highlights 45 different kinases (including JNK3) featuring methionine in both positions. (f) Distribution of these 45 kinases highlighted in the dendrogram of human protein kinases according to Manning et al.[16] by red dots. For clarity, JNK3 is represented by a green dot.

Closer inspection of the proximal amino acids in the back pocket behind MET146, reveals an unexpected, but highly interesting contact featured consistently in both chains of 4X21, however, not in 2P33. MET115, located in helix αC, adopts a different rotameric state in 4X21, forming a chalcogen bond with the sulfur electron density of MET146 from the opposite direction of the halogen bond (Figure 5c). Similar to halogens, the heavier chalcogens such as sulfur show an anisotropic electron distribution, leading to σ-holes (positive electrostatic potentials) in elongation of the $C_{\gamma/\varepsilon}$-S bond vectors.[39−43] The distance $d_{S\cdots S}$ between MET115 and MET146 corresponds with 387 pm (or 382 pm in chain B) quite well to the minima

DOI: 10.1021/jacs.5b07090
J. Am. Chem. Soc. 2015, 137, 14640−14652

reported in the literature for a similar model system (403 pm).[39] An almost linear arrangement ($\alpha_{C\gamma\text{-}S\cdots S}$ = 180°) indicates a good alignment of the σ-hole of the donor methionine with the sulfur of the acceptor methionine. We find a deviation of only $\Delta\alpha_{C\gamma\text{-}S\cdots S}$ = 26.0° for chain A and 20.3° for chain B. Additionally, a very good overlap of the donor σ-hole of MET115 with the highest electron density (lone pairs) above the C_γ−S−C_ε plane of MET146 is observed for χ_3 dihedral angle $\delta_{C\beta\text{-}C\gamma\text{-}S\text{-}C\varepsilon}$ close to −95°. Hence, the chalcogen bond donated from MET115 and the halogen bond donated from **7d** are engaged in a bivalent interaction with MET146. As shown in Figure 5c, we have therefore extended our model system by the capped MET115 (cMET115) to elucidate, how this additional interaction restricts the conformational freedom of MET146.

We rotated $\delta_{C\beta\text{-}C\gamma\text{-}S\text{-}C\varepsilon}$ in steps of 10° between −65° and −175°. All dihedral angles beyond this span clearly led to significant clashes with the ligand or MET115. We simultaneously altered the distance $d_{I\cdots S}$ from 295 to 405 pm in increments of 10 pm, giving a total of 144 single points to be evaluated. The results can be seen in Figure 5d. According to the most reasonable geometry derived from the electron density, the interaction energy amounts to approximately −28.6 kJ/mol. It should be noted that this interaction energy is only the simple adduct formation energy of the complex, not including desolvation effects or entropy contributions. Thus, the numbers cannot be interpreted as absolute, but only relative values. If the dihedral angle is changed by more than 20° toward the iodine atom ($\delta_{C\beta\text{-}C\gamma\text{-}S\text{-}C\varepsilon}$ = −75°), the mismatch of the sulfur electron density and the iodine σ-hole will be dramatically increased and steric clashes start to arise from the too close $C_\varepsilon\cdots$S contact, leading to an almost complete loss of the attractive interaction. On the basis of steric repulsion with MET115, dihedral angles of $\delta_{C\beta\text{-}C\gamma\text{-}S\text{-}C\varepsilon}$ < −165° are not possible. The interaction energy in the range −85° > $\delta_{C\beta\text{-}C\gamma\text{-}S\text{-}C\varepsilon}$ > −115° is quite similar at the given experimental distance of $d_{I\cdots S}$ = 315 pm (black line in Figure 5d). Moreover, at a larger distance, the energy surface becomes even more shallow, differing between −75° and −145° by only up to 6 kJ/mol. The chalcogen bond provides between a $\delta_{C\beta\text{-}C\gamma\text{-}S\text{-}C\varepsilon}$ of −65° and −145° an almost constant stabilization of the complex (−9.6 to −10.8 kJ/mol on a TPSS-D2/TZVPP-level of theory), quite independent of the dihedral angle.

The strength of the interaction could be further improved by a larger distance of the iodine atom (~345 pm instead of 315 pm). It is obvious from Figure 5d that the strength of the halogen bond at 315 pm will be improved or maintained up to a distance of more than 400 pm at these dihedral angles. Thus, we conclude that the experimentally determined geometry represents a still favorable, attractive interaction, however, fails to utilize the potential of the stronger σ-hole of iodine. This is due to the binding mode being clearly dominated by the tight hydrogen-bonding network to the hinge and LYS93. In addition, the too close iodine atom of **7d** increases the flexibility of C_ε of MET146, however, the rest of the residue cannot adapt, because it accepts the chalcogen bond from MET115.

We further evaluated the relative conformational strain of the MET146 side chain, when it adopts different dihedral angles. We calculated the relative energy of our cMET146 model system, when modifying $\delta_{C\beta\text{-}C\gamma\text{-}S\text{-}C\varepsilon}$. The identified torsional minimum at approximately −75° causes an almost repulsive interaction. The most plausible dihedral of −95° causes a slightly increased conformational strain of +4.0 kJ/mol, which appears to be less relevant in comparison to the gain of interaction energy (in Figure 5d). Still, combining the trend observed for the conformational strain of MET146 with the trend in the interaction energies, it appears plausible that a certain fluctuation of the χ_3 dihedral angle of MET146 of ±15° with respect to the best angle might be possible. Interestingly, in comparison to 4X21, the crystal structure of **7b** (2P33) appears to have a more well-defined electron density for C_ε, probably also correlating with the larger halogen bond distance and the smaller size of chlorine. Beside desolvation effects, this observation is one possible explanation for changes in enthalpy and entropy between these ligands, while the overall ΔG is only insignificantly different. We have calculated solvation effects using COSMO-RS (see Supporting Information, Figure S2, and Table S2) for the ligands **7a**−**d** in complex with the capped gatekeeper cMET146. The results show a good correlation between the COSMO-RS corrected and the gas phase energies (R^2 = 0.96). The desolvation energy ranges between −18.0 kJ/mol (4X21) and −19.8 kJ/mol (2P33).

CONCLUSION

We performed a matched molecular pair analysis of a series of aminopyrimidine-based JNK3 inhibitors, designed to investigate halogen bonding effects with the sulfur of MET146, the gatekeeper residue of this kinase. With a significant portion of the human kinome sharing a methionine residue as the gatekeeper, this case study is an interesting starting point for a more systematic investigation of X···S halogen bonding effects on affinity and selectivity tuning in kinase drug discovery. There are important lessons learned from this case study, which may help to guide future molecular design projects.

Despite the usual assumption that halogen bonding strength increases from chlorine to bromine to iodine, in this ligand series we encounter a plateau of affinity, reached already for chlorine (**7b**). Neither bromine (**7c**), nor iodine (**7d**) were found to provide any statistically significant advance in affinity in fluorescence polarization-based measurements or isothermal titration calorimetry. Thus, these two halogens clearly fail to reach the full potential according to the size of their σ-hole, which we have demonstrated by calculating their V_{max} value and by visualizing their electrostatic potentials. It should be emphasized that the lack of a significant improvement does not imply that they do not have greater potential for gaining affinity; however, it means that in this system other factors did not permit **7c** or **7d** to make use of this potential. On the basis of the crystal structure of **7d** in complex with JNK3 (4X21), its comparison to the original structure of **7b** in complex with JNK3 (2P33), and exploiting a systematic QM-based evaluation of parameters crucial for binding, we are able to identify these factors and to rationalize, when halogen exchange toward bromine and iodine might be a rewarding strategy and when it may not provide any advantage. Such cases, where chlorine already is the optimum can certainly be beneficial, particularly when being concerned about attrition caused by adverse effects that could be related to these heavier halogens.

From Figure 5, there is clear evidence that **7d** is held so tightly in place by the hydrogen bonding network involving the hinge (MET149, GLU147) and LYS93 that a significant displacement of the scaffold is not expectable. Despite being often considered rather flexible, methionine seems not to be able to adapt to the strongly fixed ligand by increasing the halogen bond distance from 315 pm (in the crystal structure)

DOI: 10.1021/jacs.5b07090
J. Am. Chem. Soc. 2015, 137, 14640−14652

to roughly 335 to 365 pm, where the optimum is expected according to our model calculations (shown in Figure 5d). We have shown additionally that the conformational strain of such adaptive processes should not be underestimated and can be a real liability for ligand binding. Interestingly, in our JNK3 complex with **7d**, MET146 is bivalently engaged by a halogen bond from the ligand and a chalcogen bond from MET115. This dual interaction strongly restricts the flexibility of MET146, except for the χ_3 dihedral angle. The slightly too close iodine atom in **7d** enhances the flexibility of C_ε and causes variations in χ_3 within the boundaries of the bivalent halogen/chalcogen bond, counterbalanced by the increasing conformational strain of MET146. In the context of the significant shifts between enthalpy ($\Delta\Delta H$(**7d**−**7b**) = +3.0 kcal·mol^{-1}) and entropy ($\Delta\Delta S$(**7d**−**7b**) = +11.1 cal·mol^{-1}·K^{-1}), this change in flexibility might be one relevant contribution. Of course, changes in desolvation can likewise contribute to the observed enthalpy−entropy compensation between **7b** and **7d**.[44]

As we have shown for JNK3 versus p38α, halogen bonding to the gatekeeper residue methionine can modify the selectivity profile of kinase inhibitors. This effect can, of course, depend not only on the difference between the gatekeeper residues (e.g., MET vs THR) and the discriminative way both can be targeted by halogen bonding, but it also may depend on small to subtle geometric variances in the binding site featuring the same gatekeeper. As shown in this study, the difference between an attractive and a repulsive interaction can be as small as 20−30 pm. In addition, small changes in the spherical orientation of the residue (e.g., the χ_3 dihedral angle in methionine) or deviations from a linear arrangement (σ-hole angle of 180°) by 10−30° can be sufficient to cause a substantial shift in selectivity. We prepared the gatekeeper mutants M146A, M146L, and M146T of JNK3 to scrutinize the role of the halogen bond in molecular recognition of **7b**−**d**. The strong loss of affinity for M146A suggests that an interaction with the gatekeeper residue is key to achieving high affinity for all ligands. The high similarity of the ligand binding data between M146T and p38α implies that the exchange of the gatekeeper into threonine is the major determinant of p38α/JNK3-selectivity. Apparently, none of the interaction patterns (halogen bond, hydrogen bond, dispersive/hydrophobic interaction) which threonine can form is able to compensate for the loss of the halogen bond toward methionine. In contrast, leucine as a gatekeeper of similar size can compensate, based on dispersive/hydrophobic interactions, for the loss of the methionine interaction. It shows an interesting differentiation between the halogens: the small chlorine is clearly preferred over the larger bromine and even more over iodine. Thus, preference by leucine increases with decreasing σ-hole size and decreasing volume of the halogen. Hence, although failing to modify affinity toward JNK3-wt, the choice of halogen can have an important impact on kinase selectivity.

A fascinating paradigm observed in this study is the stabilization of MET146 by the proximal MET115. The quite favorable chalcogen bond geometry restricts the motility of MET146, preventing a more efficient adaption to the too close iodine atom. Thus, this combination of chalcogen bonding partners in this position may give rise to some affinity cliffs in the structure−activity relationship (SAR) of ligand series. As highlighted in Figure 5e, when the gatekeeper is a methionine residue, the probability of a methionine as its proximal neighbor in the αC-helix of the back pocket is only 24.6%. The overall chance of two methionine residues occurring in these two positions, is only 9.3% with respect to the human kinome. Leucine has a much higher prevalence in this position of the αC-helix, however, it only can interact by forming hydrophobic contacts. Interestingly, analysis of the distribution of the 45 kinases featuring both methionine residues reveals an unequal distribution among the kinase subfamilies. While JNK3 and JNK1, both share this feature, neither JNK2, nor any other kinase in the CMGC subtree (see Figure 5f) show this combination of methionine residues. It seems to occur in small clusters of two to four closely related kinases, however, is spread rather equally across the different subfamilies, except for the Casein Kinase 1 family. Still, close proximity between two methionine residues in these two positions will not by itself guarantee formation of a chalcogen bond, as demonstrated in 2P33. However, the described paradigm may provide new opportunities for selectivity profiling in the human kinome. Clearly, more test cases and a more exhaustive comparison is needed to highlight general trends.

In a nutshell, what did we learn from this model system? Molecular design of halogen bonds in binding sites starting from molecules of high complexity[45] that comprise a substantial number of highly preoptimized interactions is certainly not trivial. Best results can be expected when the carbon···sulfur distance between the aromatic scaffold and methionine is approximately 540−560 pm and the σ-hole angle only deviates by up to 20° from linearity. It is dangerous to rely on adaptive behavior of the binding site, even with a side chain such as methionine that is usually perceived to be more flexible than most other residues. An alternative, much better strategy for such a situation is to select one of the most efficient fragments from a library such as HEFLibs (halogen-enriched fragments),[46,47] which shows an optimized halogen bond geometry with this gatekeeper and then try to grow or merge the fragment to introduce an optimized network of other interactions. Still, molecular design is a most valuable method for lead optimization. As a consequence, QM-based scoring functions for docking approaches, accounting precisely for the geometric restraints of halogen bonding[17,48] can be valuable tools complementary to the direct use of quantum chemistry or integrated QM/SQM/MM-approaches.[22,49,50]

MATERIALS AND METHODS

See Supporting Information.

ASSOCIATED CONTENT

Supporting Information

The Supporting Information is available free of charge on the ACS Publications website at DOI: 10.1021/jacs.5b07090.

Detailed information about halogen bond tuning (V_{max}), design of matched molecular pairs by quantum chemistry, synthesis procedures, biophysical characterization (DSF). Materials and methods for: QM calculations, solvation effects, organic chemistry, biochemistry, DSF, ITC, FP assay, statistical data analysis, crystallization of JNK3, data collection and structure determination of 4X21. Schemes for synthesis of **7a** and **7b** (S1), loss of regioselectivity during Suzuki cross coupling (S2), and structure of RN4646 (S3). Tables with detailed measurements of computed versus experimental complexes (S1), COSMO-RS solvation-corrected interaction energies (S2), and DSF measure-

DOI: 10.1021/jacs.5b07090
J. Am. Chem. Soc. 2015, 137, 14640−14652

ments (S3). Figures showing computed structures of MMPs in complex with JNK3 (S1), model system for calculation of solvation effects (S2), DSF curves (S3), summary of ITC results decomposed into ΔG, ΔH and $-T\Delta S$ (S4), superposition of chain A and B of 4X21 (S5), unbiased simulated-annealing omit ($F_o - F_c$) electron-density map for **7d** and MET146 in 4X21 (S6), and crystal contacts in 4X21 (S7). Detailed synthesis and characterization of compounds **3**−**7** and additional references. (PDF)

AUTHOR INFORMATION

Corresponding Author

*frank.boeckler@uni-tuebingen.de

Author Contributions

§A.L. and M.G. contributed equally.

Notes

The authors declare no competing financial interest.

ACKNOWLEDGMENTS

High performance computing resources of the BW-grid were kindly made available by the federal state of Baden-Wuerttemberg. This research was supported in part by the bwHPC initiative and the bwHPC-C5 project provided through associated computer services of the JUSTUS HPC facility at the University of Ulm. bwHPC and bwHPC-C5 (http://www.bwhpc-c5.de) are funded by the Ministry of Science, Research and the Arts Baden-Wuerttemberg (MWK) and the Germany Research Foundation (DFG). We also want to thank Prof. LoGrasso for the JNK3 plasmid.

REFERENCES

(1) Auffinger, P.; Hays, F. A.; Westhof, E.; Ho, P. S. *Proc. Natl. Acad. Sci. U. S. A.* **2004**, *101*, 16789.

(2) Politzer, P.; Lane, P.; Concha, M. C.; Ma, Y. G.; Murray, J. S. *J. Mol. Model.* **2007**, *13*, 305.

(3) Hardegger, L. A.; Kuhn, B.; Spinnler, B.; Anselm, L.; Ecabert, R.; Stihle, M.; Gsell, B.; Thoma, R.; Diez, J.; Benz, J.; Plancher, J.-M.; Hartmann, G.; Banner, D. W.; Haap, W.; Diederich, F. *Angew. Chem., Int. Ed.* **2011**, *50*, 314.

(4) Wilcken, R.; Zimmermann, M. O.; Lange, A.; Zahn, S.; Kirchner, B.; Boeckler, F. M. *J. Chem. Theory Comput.* **2011**, *7*, 2307.

(5) Wilcken, R.; Zimmermann, M.; Lange, A.; Zahn, S.; Boeckler, F. *J. Comput.-Aided Mol. Des.* **2012**, *26*, 935.

(6) Wilcken, R.; Zimmermann, M. O.; Lange, A.; Joerger, A. C.; Boeckler, F. M. *J. Med. Chem.* **2013**, *56*, 1363.

(7) Lange, A.; Zimmermann, M. O.; Wilcken, R.; Zahn, S.; Boeckler, F. M. *J. Chem. Inf. Model.* **2013**, *53*, 3178.

(8) Politzer, P.; Murray, J. S.; Clark, T. *Phys. Chem. Chem. Phys.* **2013**, *15*, 11178.

(9) Desiraju, G. R.; Ho, P. S.; Kloo, L.; Legon, A. C.; Marquardt, R.; Metrangolo, P.; Politzer, P.; Resnati, G.; Rissanen, K. *Pure Appl. Chem.* **2013**, *85*, 1711.

(10) Beno, B. R.; Yeung, K.-S.; Bartberger, M. D.; Pennington, L. D.; Meanwell, N. A. *J. Med. Chem.* **2015**, *58*, 4383.

(11) Cohen, M. S.; Zhang, C.; Shokat, K. M.; Taunton, J. *Science* **2005**, *308*, 1318.

(12) Gehringer, M.; Muth, F.; Koch, P.; Laufer, S. A. *Expert Opin. Ther. Pat.* **2015**, *25*, 849.

(13) Koch, P.; Gehringer, M.; Laufer, S. A. *J. Med. Chem.* **2015**, *58*, 72.

(14) Scapin, G.; Patel, S. B.; Lisnock, J.; Becker, J. W.; LoGrasso, P. V. *Chem. Biol.* **2003**, *10*, 705.

(15) Alam, M.; Beevers, R. E.; Ceska, T.; Davenport, R. J.; Dickson, K. M.; Fortunato, M.; Gowers, L.; Haughan, A. F.; James, L. A.; Jones, M. W.; Kinsella, N.; Lowe, C.; Meissner, J. W. G.; Nicolas, A.-L.; Perry, B. G.; Phillips, D. J.; Pitt, W. R.; Platt, A.; Ratcliffe, A. J.; Sharpe, A.; Tait, L. J. *Bioorg. Med. Chem. Lett.* **2007**, *17*, 3463.

(16) Manning, G.; Whyte, D. B.; Martinez, R.; Hunter, T.; Sudarsanam, S. *Science* **2002**, *298*, 1912.

(17) Ruff, M.; Zimmermann, M. O.; Lange, A.; Boeckler, F. M., unpublished data, 2015.

(18) Delano, W. L. *The PyMOL Molecular Graphics System*, 1.2r.1; DeLano Scientific LLC: Palo Alto, CA, 2009.

(19) Brickmann, J.; Exner, T. E.; Gimmler, J.; Lautenschläger, P.; Heiden, W.; Moeckel, G.; Zahn, D. *MOLCAD II*, V1.4; MOLCAD GmbH: Darmstadt, Germany; 2010, http://www.molcad.de.

(20) Brickmann, J.; Exner, T. E.; Keil, M.; Marhofer, R. J. *J. Mol. Model.* **2000**, *6*, 328.

(21) Lange, A.; Zimmermann, M. O.; Heidrich, J.; Exner, T. E.; Boeckler, F. M., unpublished data, 2015.

(22) Fanfrlík, J.; Kolář, M.; Kamlar, M.; Hurný, D.; Ruiz, F. X.; Cousido-Siah, A.; Mitschler, A.; Řezáč, J.; Munusamy, E.; Lepšík, M.; Matějíček, P.; Veselý, J.; Podjarny, A.; Hobza, P. *ACS Chem. Biol.* **2013**, *8*, 2484.

(23) Riley, K. E.; Murray, J. S.; Fanfrlik, J.; Rezac, J.; Sola, R. J.; Concha, M. C.; Ramos, F. M.; Politzer, P. *J. Mol. Model.* **2011**, *17*, 3309.

(24) Fresneda, P. M.; Delgado, S.; Francesch, A.; Manzanares, I.; Cuevas, C.; Molina, P. *J. Med. Chem.* **2006**, *49*, 1217.

(25) Ottoni, O.; Cruz, R.; Alves, R. *Tetrahedron* **1998**, *54*, 13915.

(26) Rossignol, E.; Youssef, A.; Moreau, P.; Prudhomme, M.; Anizon, F. *Tetrahedron* **2007**, *63*, 10169.

(27) Caldarelli, M.; Angiolini, M.; Colombo, R.; Disingrini, T.; Nuvoloni, S.; Posteri, H.; Salsa, M.; Silvagni, M., Pyrazolo-quinazolines. Eur. Pat. Appl. 2303891, April 6, 2011.

(28) Lea, W. A.; Simeonov, A. *Expert Opin. Drug Discovery* **2011**, *6*, 17.

(29) Wätzig, H.; Oltmann-Norden, I.; Steinicke, F.; Alhazmi, H. A.; Nachbar, M.; El-Hady, D. A. A.; Albishri, H. M.; Baumann, K.; Exner, T. E.; Boeckler, F. M.; El Deeb, S. *J. Comput.-Aided Mol. Des.* **2015**, *29*, 1.

(30) Munoz, L.; Selig, R.; Yeung, Y. T.; Peifer, C.; Hauser, D.; Laufer, S. *Anal. Biochem.* **2010**, *401*, 125.

(31) Ansideri, F.; Lange, A.; Elgokha, A. A.; Boeckler, F. M.; Koch, P., unpublished data, 2015.

(32) Nikolovska-Coleska, Z.; Wang, R.; Fang, X.; Pan, H.; Tomita, Y.; Li, P.; Roller, P. P.; Krajewski, K.; Saito, N. G.; Stuckey, J. A.; Wang, S. *Anal. Biochem.* **2004**, *332*, 261.

(33) *KaleidaGraph*, 4.02; Synergy Software: Reading, PA, 1986−2013.

(34) Koeberle, S. C.; Romir, J.; Fischer, S.; Koeberle, A.; Schattel, V.; Albrecht, W.; Grütter, C.; Werz, O.; Rauh, D.; Stehle, T.; Laufer, S. A. *Nat. Chem. Biol.* **2012**, *8*, 141.

(35) Xie, X.; Gu, Y.; Fox, T.; Coll, J. T.; Fleming, M. A.; Markland, W.; Caron, P. R.; Wilson, K. P.; Su, M. S. S. *Structure* **1998**, *6*, 983.

(36) Swahn, B.-M.; Huerta, F.; Kallin, E.; Malmström, J.; Weigelt, T.; Viklund, J.; Womack, P.; Xue, Y.; Öhberg, L. *Bioorg. Med. Chem. Lett.* **2005**, *15*, 5095.

(37) *Molecular Operating Environment (MOE)*, 2013.08; Chemical Computing Group Inc.: Montreal, QC, 2015.

(38) *Origin* (OriginLab: Northampton, MA).

(39) Bleiholder, C.; Werz, D. B.; Koppel, H.; Gleiter, R. *J. Am. Chem. Soc.* **2006**, *128*, 2666.

(40) Murray, J. S.; Lane, P.; Clark, T.; Politzer, P. *J. Mol. Model.* **2007**, *13*, 1033.

(41) Murray, J. S.; Lane, P.; Politzer, P. *Int. J. Quantum Chem.* **2008**, *108*, 2770.

(42) Wang, W.; Ji, B.; Zhang, Y. *J. Phys. Chem. A* **2009**, *113*, 8132.

(43) Politzer, P.; Murray, J. S.; Clark, T. *Phys. Chem. Chem. Phys.* **2013**, *15*, 11178.

(44) Ferenczy, G. G.; Keserű, G. M. *J. Chem. Inf. Model.* **2010**, *50*, 1536.

DOI: 10.1021/jacs.5b07090
J. Am. Chem. Soc. 2015, 137, 14640−14652

(45) Hann, M. M.; Leach, A. R.; Harper, G. *J. Chem. Inf. Model.* **2001**, *41*, 856.
(46) Zimmermann, M. O.; Lange, A.; Wilcken, R.; Cieslik, M. B.; Exner, T. E.; Joerger, A. C.; Koch, P.; Boeckler, F. M. *Future Med. Chem.* **2014**, *6*, 617.
(47) Wilcken, R.; Liu, X.; Zimmermann, M. O.; Rutherford, T. J.; Fersht, A. R.; Joerger, A. C.; Boeckler, F. M. *J. Am. Chem. Soc.* **2012**, *134*, 6810.
(48) Zimmermann, M. O.; Lange, A.; Boeckler, F. M. *J. Chem. Inf. Model.* **2015**, *55*, 687.
(49) Dobeš, P.; Řezáč, J.; Fanfrlík, J.; Otyepka, M.; Hobza, P. *J. Phys. Chem. B* **2011**, *115*, 8581.
(50) Brahmkshatriya, P. S.; Dobes, P.; Fanfrlik, J.; Rezac, J.; Paruch, K.; Bronowska, A.; Lepsik, M.; Hobza, P. *Curr. Comput.-Aided Drug Des.* **2013**, *9*, 118.

DOI: 10.1021/jacs.5b07090
J. Am. Chem. Soc. 2015, 137, 14640−14652